RSC Advances

ROYAL SOCIETY OF CHEMISTRY

www.rsc.org/advances

RSC Advances

ARTICLE

A Composite Electrodeposited PbO_2/SnO_2 Positive Electrode Material for Hybrid Supercapacitors

Received 00th January 2015,
Accepted 00th January 2015

DOI: 10.1039/x0xx00000x

www.rsc.org/

Yuanyuan Dan[a], Haibo Lin[*b], Lizhuang Chen[**a], Li Zhang[a], Jing Su[d], Huijuan Yue[c], Xingwei Cai[a]

PbO_2/SnO_2 composites have been prepared by composite electrodeposition method from Pb^{2+} solution containing different amounts of suspended nano-SnO_2 particles. Chemical composition, crystal structure and surface morphology of the composites were characterized by X-ray photoelectron spectroscopy (XPS), X-ray diffraction (XRD) and scanning electron microscopy (SEM). The results indicate that the composite composed of rutile phase SnO_2 and β-PbO_2 is rough and porous. The R_F of the PbO_2/SnO_2 composite is approximately 10 times higher than that of pure PbO_2 electrode. The electrochemical behavior and the capacitance performance of the composite are determined by cyclic voltammetry (CV), electrochemical impedance spectroscopy (EIS), and charge-discharge test. The composite shows a high specific capacitance up to 208 $F{\cdot}g^{-1}$, which is four times the specific capacitance of pure PbO_2 and two times that of pure SnO_2.

Introduction

With fossil energy crisis and worsening environmental pollution, the demand for environmentally friendly and high-performance supercapacitors has been increasing.[1] Hybrid supercapacitors have become a research hot spot because they have both high specific energy and high specific power. A hybrid supercapacitor usually consists of an electrode similar to a rechargeable-battery electrode of active materials with faradaic pseudocapacitance, and an activated carbon electrode that interfaces with the electrolyte in the double-layer region.[2,3] RuO_2 and IrO_2 [4,5] with large specific capacitance and good cyclic stability values are the best choices for the positive electrode; however, both are expensive. Therefore, low-cost metal oxides should be explored and studied as alternative electrodes.

Recently, PbO_2 has been used as the positive electrode in hybrid supercapacitors.[6] For example, super-large dendrites composed of trigonal PbO_2 nanoplates were synthesized by electrodeposition and tested as potential materials for electrochemical device applications.[7] Bartlett et al. reported a simple method to prepare nanostructured macroporous α- and β-PbO_2 films with arrays of spherical pores arranged in a highly ordered close-packed structure for supercapacitors.[8] Gao et al. employed a pulse current technique to prepare PbO_2 thin films as a positive electrode in a PbO_2/AC hybrid capacitor.[9,10] Lin et al. found that the capacitance of PbO_2 prepared by galvanostatic electrodeposition on three-dimensional porous titanium was improved as a result of the electrochemical active surface area and small charge transfer resistance.[11,12] All the results to date suggest that the PbO_2/AC in a sulfuric acid system is considered to be more economically viable and can yield improved performance of power and life span compared with lead-acid batteries. Nevertheless, the capacitance of pure PbO_2 is low.

Doping other elements into PbO_2 has been found effective in improving the specific capacity, activity and utilization rate of PbO_2.[13,14,15] Recently, Sivakumar et al. prepared the PbO_2–CNT composite as a positive electrode in an asymmetric hybrid supercapacitor.[16] This system exhibited a maximum power density and a maximum energy density of 1200 $W{\cdot}Kg^{-1}$ and 65 $Wh{\cdot}Kg^{-1}$, respectively, at a current density of 2 $A{\cdot}g^{-1}$. In our previous work,[17] nano-Mn_3O_4 + PbO_2 composite electrode materials were prepared by anodic composite electrodeposition in Pb^{2+} plating solution containing suspended nano-Mn_3O_4 particles. Such composite exhibited a high specific capacitance of up to 338 $F{\cdot}g^{-1}$.

In the current study, we choose nano-SnO_2 particles as additions doped into the PbO_2 matrix to synthesize PbO_2/SnO_2 composite. As additions, nano-SnO_2 has two merits: (1) it has high activity and high specific capacitance,[18] and (2) the lattice structures of SnO_2 and PbO_2 are both rutile type. Therefore, the PbO_2/SnO_2 composite can provide higher specific capacity and better stability than pure PbO_2. The composite electrodeposition method is adopted to prepare the PbO_2/SnO_2 composite onto the Ti plate. This method is one of the simplest and most effective synthesis routes for composites.[19, 20] The electrolyte for the electrodeposition contains suspended nano-SnO_2 particles. Variable amounts of nano-SnO_2 particles become dispersed and embedded into the PbO_2-matrix-form electrolyte. Then, the composition, structure, and morphology of the composite material are characterized by physical

[a] School of Environmental and Chemical Engineering, Jiangsu University of Science and Technology, Zhenjiang, 212003, P.R. China. E-mail: chenlizhuang1977@sina.com; clz1977@sina.com.
[b] College of Chemistry, Jilin University, Changchun 130012, P.R.China. E-mail: DanielEducation@hotmail.com; lhb910@jlu.edu.cn.
[c] State Key Laboratory of Inorganic Synthesis and Preparative Chemistry, College of Chemistry, Jilin University, Changchun 130012, P.R. China.
[d] School of Chemistry and Chemical Engineering, Guangxi University, Nanning, Guangxi, 530004, P.R. China

† Electronic Supplementary Information (ESI) available: [details of any supplementary information available should be included here]. See DOI: 10.1039/x0xx00000x

tests. The electrochemically effective area ratio (R_F) and capacitance of the PbO_2/SnO_2 composite in acid solution are studied through electrochemical tests. Accordingly, general knowledge of the capacitance performance and the charge-discharge mechanism of the PbO_2/SnO_2 composite in the acid-medium supercapacitor are acquired. These results provide the foundation for employing the PbO_2/SnO_2 composite as a positive electrode in an asymmetric hybrid supercapacitor.

Experimental

Preparation of nano-SnO_2 particles

All chemicals used in the experiment were of analytical grade and were used without further purification. In a typical experimental process, at room temperature, 1 mmol of oxalic acid and 1 mmol of cetyl trimethyl ammonium bromide (CTAB) were dissolved in 25 mL of deionized water, and then 1 mmol of $SnCl_2{\cdot}2H_2O$ was added into the solution under continuous stirring until the color of the solution turned to milky white. Then, the mixture solution was transferred into a Teflon-lined stainless-steel autoclave (100 mL) and was subjected to heat treatment at 160 °C for 6 h. After the autoclave cooled naturally to room temperature, the products were collected by centrifugation, washed thrice with deionized water and then with anhydrous ethanol. Finally, the nano-SnO_2 particles were vacuum-dried for 8 h at 50 °C.

The SnO_2 nano-particles have good suspension property in the plating solution, since they were modified by CTAB in the synthesis process.

Preparation of PbO_2/SnO_2 composite

The Ti substrate with a thickness of 1 mm was abraded with emery paper and corroded in HCl solution. The SnO_2–Sb_2O_5 layer was prepared on the Ti substrate by thermal decomposition method.[21]

As shown in the schematic in Fig. 1(a), the electrolytic deposition of composite oxides was performed in a three-electrode electrolytic cell with an aeration pipe without a diaphragm. The working and counter electrodes were Ti/SnO_2–Sb_2O_5 (1 cm × 1 cm) and Ti/RuO_2–TiO_2 (2 cm × 2 cm), respectively. A KCl-saturated calomel electrode (SCE) was used as reference. The 100 mL of electrolytic solution consisted of 0.1 mol·L^{-1} $Pb(NO_3)_2$ and suspended nano-SnO_2 particles with different concentrations. The nano-SnO_2 particle concentrations (C) were 0, 2, 4, 6, 8, and 10 mmol·L^{-1}. The pH value of the electrolyte was approximately 3–4.

The suspension of the nano-SnO_2 particles in the cell was sonicated for 5 min. All compartments were filled with the same electrolytic solution. The suspension in the central compartment was stirred by air blowing. Electrolyses were performed under constant potential control of 1.45 V for 1 h by a potentiostat/galvanostat (Model 8511C, Eternal Electrochemical Instrument Company, China). After deposition, the working electrodes were rinsed with distilled water. The surface schematic diagram of the working electrodes is shown in Fig. 1b. The deposition was approximately 10 mg, which was obtained by weight difference method.

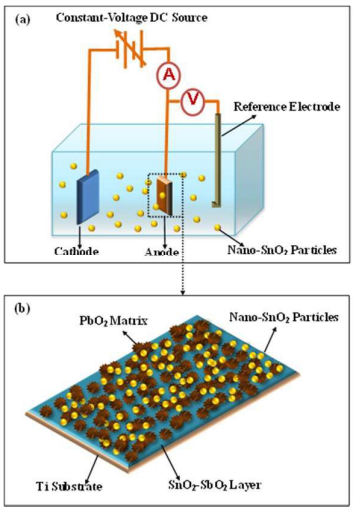

Fig. 1 Schematics showing the composite electrodeposition of PbO_2/SnO_2 (a) and the PbO_2/SnO_2 electrode surface (b).

Preparation of active carbon cathode

The active carbon (AC) electrodes were prepared by mixing the YP17 activated carbon from Kuraray with 5 wt.% conductive acetylene black and 5 wt.% polytetrafluoroethylene emulsion to form a slurry. The slurry was filtered with Ti mesh (2 cm × 2 cm), dried, and roll-pressed to approximately 50 mg.

Characterization

The morphology and particle size of nano-SnO_2 particles were analyzed by transmission electron microscopy (TEM) with a JEOL JEM-1200EX transmission electron microscope operating at 100 kV (Japan).

The crystalline phase of the synthesized composite was identified by X-ray diffraction (XRD) using a Ragaku D/max-2500 diffractometer (Japan) with Cu-Kα radiation operating at 40.0 kV and 200.0 mA (λ = 1.541784 Å). Composition analysis was conducted by X-ray photoelectron spectroscopy (XPS) using Thermo Scientific ESCALAB 250 X-ray photoelectron spectrometer with monochromatized radiations (Al, Kα) (USA). Scanning electron microscopy (SEM), which was performed on a JSM-6700F field-emission scanning electron microscope (Japan), was employed to check the morphologies of the composite. Zeta potentials of the particles were measured with a ZetaPALS apparatus (Brookhaven Instrument, USA).

Cyclic voltammetry (CV), electrochemical impedance spectroscopy (EIS), and charge-discharge test were performed on an EG&G Princeton Applied Research model 2273 potentiostat/galvanostat controlled by PowerSuite software (USA). In all the tests, 1 mol·L^{-1} H_2SO_4 solution was the medium solution, an SCE was the reference electrode, an AC electrode was the counter electrode, and the prepared composite electrode was the working electrode.

Results and discussion

Composition, structure and morphology of PbO_2/SnO_2

The XRD patterns of SnO_2, pure PbO_2, and the PbO_2/SnO_2 composite are illustrated in Fig. 2a. All diffraction peaks can be indexed to a rutile-phase SnO_2 (JCPDS Card 24–0734) and pure β-PbO_2 (JCPDS Card 41–1492) in good agreement. No additional peaks of other phases have been detected in the XRD patterns, indicating high purity and good crystallinity of the SnO_2 and pure PbO_2 products. By comparison, the XRD pattern of the PbO_2/SnO_2 composite shows the distinct diffraction peaks belong to rutile-phase SnO_2 and β-PbO_2, respectively. The results indicate that the composite is composed of rutile-phase SnO_2 and β-PbO_2.

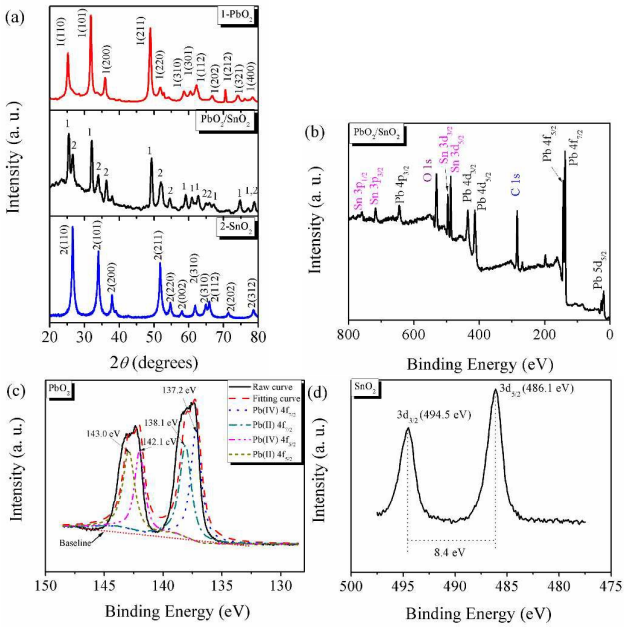

Fig. 2 The XRD patterns of SnO_2 nanoparticles, PbO_2, and PbO_2/SnO_2 (a). The X-ray photoelectron spectra of PbO_2/SnO_2 (b), and the narrow scans of Pb4f (c), and Sn3d (d).

X-ray photoelectron spectroscopy (XPS) was further employed to demonstrate the element valence state and chemical composition of the PbO_2/SnO_2 composite. All the measurements were conducted with reference to the C1s binding energy (BE, 284.6 eV) as an internal standard. The representative XPS spectrum of a typical PbO_2/SnO_2 composite over a wide range of binding energies is shown in Fig. 2b; signals of Sn, Pb, O, and C elements are observed. The XPS of Pb4f and Sn3d binding energies for the composite are shown in Fig. 2c and 2d, respectively.

The detailed spectra of Pb are shown in Fig. 2c. Two peaks centered at 137.7 eV and 142.5 eV are observed and can be attributed to the $Pb4f_{7/2}$ and $Pb4f_{5/2}$ binding energies, respectively. These results are consistent with the findings reported by other researchers.[22] The $Pb4f_{7/2}$ and $Pb4f_{5/2}$ peaks can be further divided respectively into two separate peaks at 137.2, 138.1 eV and 142.0, 146.8 eV, which could be attributed respectively to Pb(IV) $4f_{7/2}$,[23] $4f_{5/2}$[24] and Pb(II) $4f_{7/2}$,[25] $4f_{5/2}$.[26] The binding-energy difference between $4f_{7/2}$ and $4f_{5/2}$ is almost 4.9 eV, which is similar to that reported in the literature.[22] The analyses show that the valence states of Pb in our sample are +2 and +4. According to the XRD analyses, the PbO_2 of the composite, which consists of Pb(II) and Pb(IV), is β-PbO_2, which is consistent with the previously reported results.[27]

As shown in Fig. 2d, peaks located at 494.5 eV and 486.1 eV can be attributed to $Sn3d_{3/2}$ and $Sn3d_{5/2}$, whose BE values agree well with those reported in the literature.[28,29] The spin–orbit splitting is the difference between the BE values of $Sn3d_{3/2}$ and $Sn3d_{5/2}$ levels. Similar to the tin oxide reported in the literature, the observed spin-orbit splitting is 8.4 eV,[30] indicating that the valence state of Sn is +4. The analyses show that pure SnO_2 indeed exists. The XRD and XPS analyses clearly show that the composites consist of SnO_2 and β-PbO_2.

The PbO_2/SnO_2 composites with different compositions were prepared by adjusting the concentrations (C) of nano-SnO_2 particles in the plating solution. The compositions of the deposits were identified by XPS analyses using Eq. (1). The atomic ratios of Sn to Pb in the composites are listed in Table 1.

$$P_{Sn} = N_{Sn} / (N_{Sn} + N_{Pb} + N_O) \quad (1)$$

where P_{Sn} is the Sn atom fraction, N_{Sn} is the number of Sn atoms in the composite, N_{Pb} is the number of Pb atoms in the composite, and N_O is the number of O atoms in the composite.

The results show that P_{Sn} increases with increasing C. However, the adsorption of SnO_2 on the substrate has reached its maximum and has plateaued. The maximum value of P_{Sn} is 10.72 at.% when C is 10 mmol·L^{-1}. The co-deposition is limited by the formation of PbO_2.[31]

Table 1 Surface composition of PbO_2/SnO_2 composites determined by XPS and the corresponding concentration of nano-SnO_2 particles in the plating suspension (C)

Materials	C mmol·L^{-1}	P_{Sn} at.%	P_{Pb} at.%	Sn:Pb	C_{dl} μF·cm^{-2}	R_F
PbO_2	0	0	33.33	0:1	69.40	1.15
PbO_2/SnO_2	2	3.17	27.82	0.11:1	180.64	3.01
	4	5.71	27.22	0.21:1	225.3	3.75
	6	9.31	26.31	0.35:1	406.4	6.77
	8	10.07	25.65	0.39:1	603.5	10.06
	10	10.72	24.58	0.43:1	654.7	10.91

The TEM images of the nano-SnO_2 particles shown in Fig. 3a indicate that the size of the nanoparticles is approximately 5–8 nm. The SEM images of the different PbO_2/SnO_2 composite electrode surfaces are presented in Fig. 3c–3f.

Fig. 3c shows that PbO_2 grains exhibit a pyramidal feature, have a diameter of approximately 5 μm, and are closely packed on the substrate surface. In Fig. 3d and 3f, the pyramidal grains have disappeared on the electrode surface, and the PbO_2/SnO_2 composite grains have become smaller as the level of doping of nano-SnO_2 particles is increased. As shown in Fig. 3g, when the P_{Sn} is 10.72 at.%, the surface of the PbO_2/SnO_2 composite electrode is porous, and its surface roughness is increased. Furthermore, a considerable number of clubbed crystals are found on the surface. The results reveal that the specific surface area and porosity of the composite electrode material increase with increasing nano-SnO_2 doping content.

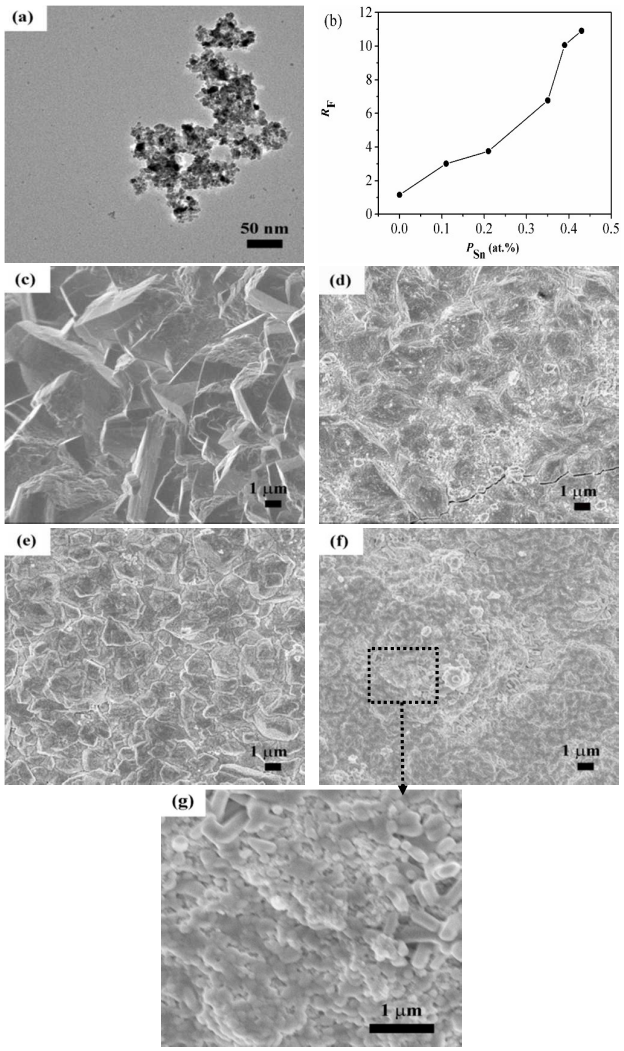

Fig. 3 TEM images of SnO_2 nanoparticles (a). Dependence of R_F on P_{Sn} (b). SEM images of PbO_2/SnO_2 composites. P_{Sn}=0 at.% (c), P_{Sn}=3.17 at.% (d), P_{Sn}=9.31 at.% (e), P_{Sn} =10.72 at.% (f), partial enlarged detail of the SEM for P_{Sn} =10.72 at.%.

The electric double-layer capacitance method[32] was used to further clarify the porosity of the PbO_2/SnO_2 composite. The electrochemically effective area ratio (R_F) values of the composite were estimated by the following equation:

$$R_F = C'_{dl} / C^0_{dl} \quad (2)$$

where C'_{dl} is the observed electric double-layer capacitance of the composite and C^0_{dl} is the electric double-layer capacitance of a smooth oxide (60 μF·cm^{-2}). The values of C'_{dl} were obtained from EIS tests. Table 1 and Fig. 3b demonstrate the relationship between R_F and P_{Sn}.

As shown in Table 1 and Fig. 3b, the RF of the PbO_2/SnO_2 composite is approximately 10 times higher than that of the PbO_2 electrode without nano-SnO_2 to the maximal degree. The results are in accordance with the SEM analysis results (Fig. 3c–3f), indicating that the R_F and porosity of the composite are proportional to P_{Sn}.

The structural properties of the composite, such as porosity, grain size, and grain geometry, as well as specific surface area, are significantly influenced by the embedded nano-SnO_2 particles. The ξ of the nano-SnO_2 particles in the planting solution is -4.16 eV. This result indicates that the particles are preferentially adsorbed on the electrode surface as an effect of the electric field.[31] Consequently, the nano-SnO_2 particles are entrapped within the PbO_2 deposit and then become new crystal nuclei. Therefore, the growth rate of the crystal nuclei increases, whereas the growth rate of the PbO_2 grains decreases. At the same time, the crystal growth in the horizontal direction is restrained by the nano-SnO_2 occupying the active site. The crystal growth accelerates in the vertical direction. The two-dimensional growth of the grains is unable to cover the electrode surface. This result indicates that the size of the grains decreases and the electrode surface porosity increases.

Capacitance performance of PbO_2/SnO_2

The electrical behaviors of pure PbO_2, the PbO_2/SnO_2 composite, and pure SnO_2 were tested using CV. Fig. 4 shows the cyclic voltammograms of these materials at a scan rate of 25 mV/s versus that of the reference SCE in 1 mol·L^{-1} H_2SO_4 solution.

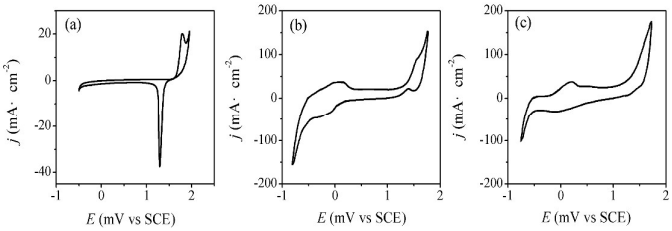

Fig. 4 Cyclic voltammorgrams of PbO_2 (a), PbO_2/SnO_2 (b) and SnO_2 (c) electrode materials in 1mol·L^{-1} H_2SO_4 solution at 25 mV·s^{-1}.

Fig. 4a illustrates the typical cyclic voltammogram of PbO_2 in a H_2SO_4 solution. The cyclic voltammogram of PbO_2 is characterized by a pair of redox peaks in the potential range of 1.2–1.8 V. This pair of peaks could be attributed to the $PbO_2/PbSO_4$ redox reaction.[33] The cyclic voltammagram of SnO_2 is presented in Fig. 4c. The oxidation peak at 0.5 V is attributed to the oxidation of SnO formed in the reverse scan, and the reduction peak at 0 V is attributed to the reduction of SnO_2 formed in the forward scan. The cyclic voltammogram of the PbO_2/SnO_2 composite in H_2SO_4 solution is shown in Fig. 4b.

The cyclic voltammogram of the PbO_2/SnO_2 composite is characterized by two pairs of peaks in the potential range of -0.2 V to 1.8 V. One pair of close-to-ideal reversible redox peaks appears at approximately 1.6–1.8 V. The cathodic peak at 1.6 V is attributed to the reduction of PbO_2, and the anodic peak at 1.8 V is attributed to the oxidation of $PbSO_4$, which is expressed as follows:

$$PbSO_4 + 2H_2O \leftrightarrow PbO_2 + HSO_4^- + 3H^+ + 2e^- \quad (3)$$

Almost of the nano-SnO_2 particles are wrapped by the PbO_2 deposit. However, the reactions involving SnO_2 react inside the PbO_2/SnO_2 composite because the electrons transfer from PbO_2 to nano-SnO_2 by an intimate electronic interaction. According to the mechanism of nano-SnO_2 charge and discharge processes,[34] the pair of peaks in the potential range of -0.5 V to 0.5 V could be attributed to Sn(II)/Sn(IV). The corresponding electron-transfer reaction is illustrated as follows:

$$[PbO_2 - SnO_2] + 2H^+ + 2e^- \leftrightarrow [PbO_2 - SnO] + H_2O \quad (4)$$

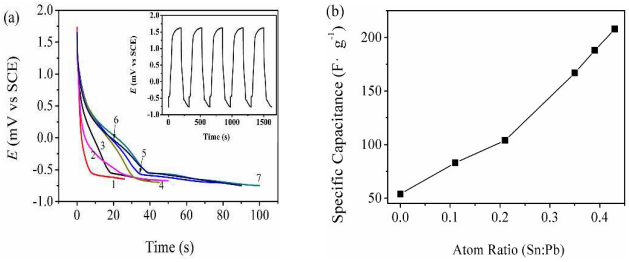

Fig. 5 Discharge curves for different electrode materials in 1mol·L^{-1} H_2SO_4 solution at 50 mA·cm^{-2} (a); The inset in (a) is charge-discharge curves for PbO_2/SnO_2 composite (P_{Sn}=10.72 at.%) in 1mol·L^{-1} H_2SO_4 solution at 10 mA·cm^{-2}. (Note: PbO_2 (1), SnO_2 (2), PbO_2/SnO_2 with P_{Sn}=3.17 at.% (3), P_{Sn}=5.71 at.% (4), P_{Sn}=9.31 at.% (5), P_{Sn}=10.07at.% (6), P_{Sn}=10.72 at.% (7).) Specipc discharge capacitance versus atom ratio (Sn:Pb) for the composites in 1 mol·L^{-1} H_2SO_4 solution (b).

The specific capacitances of the PbO_2/SnO_2 composites with different compositions were investigated through a charge-discharge test. The discharge behaviors of the PbO_2/SnO_2 composites in 1 mol·L^{-1} H_2SO_4 solution at a constant current density of 50 mA·cm^{-2} are shown in Fig. 5a. The discharge specific capacitance of the PbO_2/SnO_2 composite was calculated according to the following equation:

$$C_g = \frac{I \cdot t}{\Delta E \cdot m} \quad (5)$$

where C_g is the discharge specific capacitance, I is the constant current (50 mA·cm^{-2}), t is the time for discharging, ΔE is the observed change in the voltage, and m is the total mass of the active materials (10 mg) of different electrode materials. The details of the specific capacitance calculated from Fig. 5a are summarized in Table 2.

Table 2 Specific capacitances of the materials with different composition at 50 mA·cm^{-2} in 1 mol·L^{-1} H_2SO_4.

Materials	P_{Sn} at.%	P_{Pb} at.%	Sn:Pb	C_g F·g^{-1}
PbO_2	0	33.33	0:1	54
nano-SnO_2	33.33	~	~	102
PbO_2/SnO_2	3.17	27.82	0.11:1	83
	5.71	27.22	0.21:1	104
	9.31	26.31	0.35:1	167
	10.07	25.65	0.39:1	188
	10.72	24.58	0.43:1	208

In Fig. 5a, discharge curves 1 and 2 belong to pure PbO_2 and SnO_2, respectively. Discharge curve 1 declines rapidly, whereas discharge curve 2 decreases slowly in the potential range of -0.5 V to 0 V. The specific capacitance values of PbO_2 and SnO_2 are approximately 54 F·g^{-1} and 102 F·g^{-1}, respectively. These results are in agreement with the CV analysis results shown in Fig. 4a and 4c. As shown in Fig. 5a, discharge curves 3–7 belong to the PbO_2/SnO_2 composites with different compositions. The electrochemical window of the PbO_2/SnO_2 composites reaches approximately 2.5 V. The discharge process for the PbO_2/SnO_2 composites could be divided into three stages. In addition, the slopes of the discharge curves of the composites decrease with increasing P_{Sn}. The first stage is 1.75–0.5 V, which is characterized by a steep depression discharge curve. The next stage shows a smooth and slowly decreasing discharge interval around 0.5 V to -0.5 V. The slope of the discharge curve in this interval decreases with the increasing concentration of doped nano-SnO_2. Furthermore, this discharge interval significantly contributes to the capacitance of the PbO_2/SnO_2 composite, which results from the charge-discharge reaction shown in Eq. (4)). After the stable discharge interval, the discharge curve continues to decline to -0.75 V, constituting the third stage. The inset in Fig. 5a is charge-discharge current versus time for the PbO_2/SnO_2 composite (P_{Sn} = 10.72 at.%) in 1 mol·L^{-1} H_2SO_4 solution at 50 mA·cm^{-2}. The result reveals that the PbO_2/SnO_2 composite has a stable capacitance over several life cycles.

As shown in Table 2, the specific capacitance of the PbO_2/SnO_2 composite with 5.71 at.% Sn is twice as large as the pure PbO_2 specific capacitance, which increases to 104 F·g^{-1} because of the embedded nano-SnO_2 particles in the composition. When P_{Sn} is at 10.72 at.%, the specific capacitance of the PbO_2/SnO_2 composite shows a high specific capacitance of up to ~208 F·g^{-1}, which is four times the specific capacitance of pure PbO_2 and two times that of pure SnO_2. Fig. 5b shows the relationship curve between the specific capacitance and the atom ratio (Sn:Pb) of the composite. When the Sn:Pb ratio is 0.11, 0.21, 0.35, 0.39, and 0.43, the corresponding specific capacitance values of the PbO_2/SnO_2 composite are 83, 104, 167, 188, and 208 F·g^{-1}, respectively. Research shows that the specific capacitance of the composite increases as P_{Sn} increases.

The high capacitance of the PbO_2/SnO_2 composite in the current study can be attributed to the intimate electronic interaction and synergistic effect between PbO_2 and nano-SnO_2. The nano-SnO_2 particles in the bulk phase of the composite can effectively and rapidly store and release a charge through the highly conductive PbO_2. The physical continuity of the active material facilitates the electron conduction from the electrode surface to the current collector. They can lend good storage performance to the composite. Furthermore, the PbO_2/SnO_2 composite material has a large electrochemically effective area and high porosity. Thus, medium transmission distance can be ignored, and the restrictions on medium diffusion can be reduced. Large surface area facilitates the electrochemical reaction at the electrode/solution interface and improves the utilization ratio of PbO_2.

To further interpret the characteristics of the PbO_2/SnO_2 composite, EIS was performed in 1 mol·L^{-1} H_2SO_4 solution at 0.5 V, and the EIS data for the PbO_2/SnO_2 composite were compared with those of the reference SCE. The EIS data are presented in a Nyquist plot in Fig. 6. Fig. 6a shows the original curve and the fitting as well as the equivalent electric circuit (inset) for the EIS spectrum. As shown in Fig. 6a, the internal resistance, R_s, of the cell is obtained at ~0.5 Ω from the high-frequency intercept on the real axis; R_s includes the resistances of the electrolyte and the active material, and a large contribution from the discharge product of $PbSO_4$. The small internal resistance reveals that the composites have excellent electrical conductivities. The complex plane plot for the PbO_2/SnO_2 composite contains two frequency regions. The plot displays an imperfect half semicircle in the 10–4.3 KHz region (Fig. 6b). It belongs to the charges transfering from the solution to the electrode surface for double layer capacitance. The double-layer

capacitance (C_{dl}) and faraday leakage resistance (R_{F1}) are given by fitting the curve of the imperfect half semicircle. The fitted value of the C_{dl} is 654.7 μF·cm^{-2}. In the 4.3 KHz to 10 mHz region (Fig. 6c), the quadrant arc is observed to have a 45° sloping line. This quadrant arc belongs to the charges for the faraday reaction to contributing faradaic pseudocapacitance. The pseudocapacitance (C_{φ}) is 1296 mF·cm^{-2} obtained by fitting and calculating. This charge-transfer process occurs between the solution & PbO_2, the solution & SnO_2, and SnO_2 & PbO_2.This resultes indicates that two charge-transfer controlled processes occur and the double-layer capacitance contributes minimally to the total capacitance, that is, the capacitance of the composite is mainly the result of the faradaic reaction. The 45° sloping line, which is unrelated to frequency, indicates that the PbO_2/SnO_2 composite is once again porous.[35] As the composite is porous, the electrolyte diffuses not only onto the electrode surface but also into the pores of the composite.

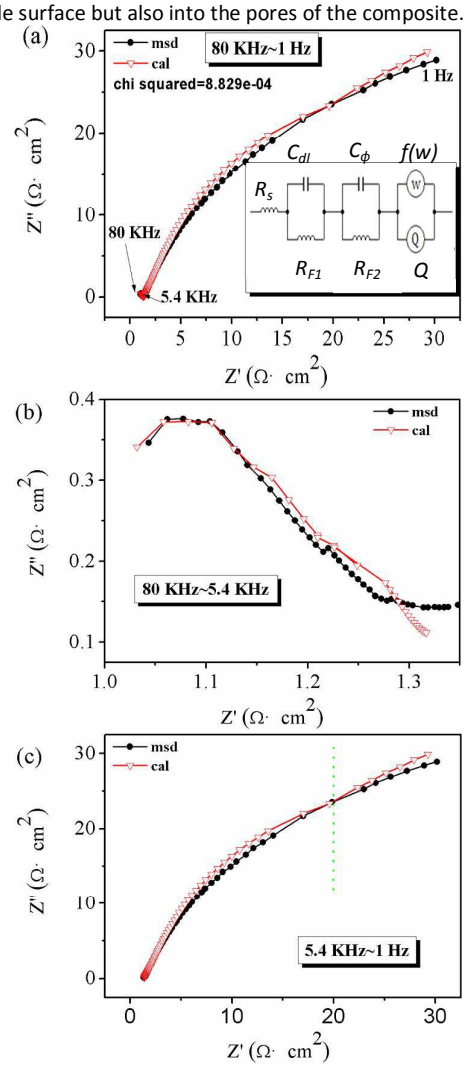

Fig. 6 EIS of PbO_2/SnO_2 composite (P_{Sn}=10.72 at.%) in 1mol·L^{-1} H_2SO_4 solution at 0.5 V versus SCE (the inset is the equivalent electric circuit for the EIS) (a), and the magnifications of 10–4.3 KHz region (b), 4.3–10mHz region (c). R_s: inner resistance; R_{F1}: Faraday leakage resistance; R_{F2}: Faraday reaction resistance; *f(w)*: diffusion impedance; C_{dl}: double electric layer capacitance; C_{φ}: Pseudo capacitance.

Conclusions

The PbO_2/SnO_2 composite electrode materials with different compositions were successfully prepared by anode-composite deposition method from the Pb^{2+} plating solution containing suspended nano-SnO_2 particles. The PbO_2/SnO_2 composite is composed of rutile-phase SnO_2 and *β*-PbO_2. The composite is porous and has a maximum electrochemically effective area ratio (R_F) of 72. The PbO_2/SnO_2 composite has a high specific capacitance of up to ~208 F·g^{-1}, which is attributed to the intimate electronic interaction and synergistic effect between PbO_2 and nano-SnO_2, and the porous structure of the composite. The PbO_2/SnO_2 composite can be further explored as a high-capacitance and low-cost positive electrode material for hybrid supercapacitor applications.

Acknowledgements

The authors are grateful for the support provided by the National Natural Science Foundation of China (No.51502117, No.21201087, and No.21573093), Jiangsu Provincial Natural Sciences Foundation of China (No.BK20130460, No.BK20131244), Guangxi Nature Science Foundation (No.2012GXNSFBA053019), and open fund of State Key Laboratory of Inorganic Synthesis and Preparative Chemistry (No.2014-14).

References

1 F. X. Wang, S.Y. Xiao, Y.Y. Hou, C. L. Hu, L. L. Liu and Y. P. Wu, *RSC Adv.*, 2013, **3**, 13059.
2 B. E. Conway, *J. Electrochem. Soc.*, 1991, **138**, 1539.
3 J. P. Zheng, P. J. Cygan and T. R. Jow, *J. Electrochem. Soc.*, 1995, **142**, 2699.
4 Z. Gui, E. Gillette, J. Duay, J. K. Hu, N. Kim and S. B. Lee, *Phys. Chem. Chem. Phys.*, 2015, **17**, 15173.
5 S. Ferro, D. Rosestolato, C. A. Martinez-Huitle and A. D. Battisti, *Electrochim. Acta*, 2014, **148**, 85.
6 S. A. Kazaryan, S. N. Razumov, S. V. Litvinenko, G. G. Kharisov and V. I. Kogan, *J. Electrochem. Soc.*, 2006, **153**, 1655.
7 L. X. Ding, F. L. Zheng, J. W. Wang, G. R. Li, Z. L. Wang and Y. X. Tong, *Chem. Commun.*, 2012, **48**, 1275.
8 P. N. Bartlett, T. Dunford and M. A. Ghanem, *J. Mater. Chem.*, 2002, **12**, 3130.
9 N. F. Yu, L. J. Gao, *Electrochem. Commun.*, 2009, **11**, 220.
10 N. F. Yu, L. J. Gao, S. H. Zhao and Z. D.Wang, *Electrochim. Acta*, 2009, **54**, 3835.
11 W. L. Zhang, H. B. Lin, H. S. Kong, H. Y. Lu, Z. Yang and T. T. Liu, *Electrochim. Acta*, 2014, **139**, 209.
12 W. L. Zhang, H. B. Lin, H. S. Kong, H. Y. Lu, Z. Yang and T. T. Liu, *Int. J. Hydrogen Energy*, 2014, **39**, 17153.
13 E. A. Dalchiele, S. Cattarin, M. Musiani, U. Casellato and P. Guerriero, *J. Appl. Electrochem.*, 2000, **30**, 117.
14 H. Lin, J. F. Niu, J. Xu, Y. Li, Y. H. Pan, Elec*trochim. Acta*, 2013, **97**, 167.
15 J. F. Niu, H. Lin, C. Gong, X. M. Sun, *Environ. Sci. Technol.*, 2013, **47**, 14341.
16 M. S. Soumya, G. Binitha1, P. Praveen, K. R. V. Subramanian, Y. S. Lee, V. Shantikumar Nair and N. Sivakumar, *J. Nanosci.*

Nanotechno., 2015, **15**, 703.
17 Y.Y. Dan, H. B. Lin, X. L. Liu, H. Y. Lu, J. Z. Zhao, Z. Shi and Y. P. Guo, *Electrochim. Acta*, 2012, **83**, 175.
18 Y. H. Zhu, E. H. Liu, Z. Y. Luo, T. T. Hu, T. T. Liu, Z. P. Li and Q. L. Zhao, *Electrochim. Acta*, 2014, **118**, 106.
19 C. T. J. Low, R. G. A. Wills and F. C. Walsh, *Surf. Coat. Technol.*, 2006, **201**, 371.
20 S. Cattarin, I. Frateur, P. Guerriero and M. Musiani, *Electrochim. Acta*, 2000, **45**, 2279.
21 A. Brian, T. Min and C. Aicheng, *Electrochim. Acta*, 2008, **54**, 1491.
22 J. Morales, G. Petkova, M. Cruz and A. Caballero, *J. Power. Sources.*, 2006, **158**, 831.
23 K. S. Kim, T. J. O'Leary and N. Winograd, *Anal. Chem.*, 1973, **45**, 2214.
24 L. Z. Zhao, *Solid State Commun.*, 1995, **94**, 857.
25 Y. Ohno, *Phys. Rev. B*, 1991, **44**, 1281.
26 M. E. Ekman, J. W. Anderegg and G. L. Schrader, *J. Catal.*, 1989, **117**, 246.
27 D. P. Guo, C. Robinson and J. E. Herrera, *Environ. Sci. Technol.*, 2014, **48**, 12525.
28 R. Shiratsuchi, K. Hongo, G. Nogami and S. Ishimaru, *J. Electrochem. Soc.*, 1992, **139**, 2544.
29 D. Shuttleworth, *J. Phys. Chem.*, 1980, **84**, 1629.
30 C. H. Wang, C. L. Shao, X. T. Zhang and Y. C. Liu, *Inorg. Chem.*, 2009, **48**, 7261.
31 N. Guglielmi, *J. Electrochem. Soc.*, 1972, **119**, 1009.
32 S. Levine and A. L. Smith, *Faraday Soc.*, 1971, **52**, 290.
33 A. Hrussanova, L. Mirkova and T. S. Dobrev, *Hydrometallurgy*, 2001, **60**, 199.
34 J. H. Shin, H. M. Park and J. Y. Song, *J. Alloys Compd.*, 2013, **551**, 451.
35 R. de Levie, *Electrochim. Acta*, 1963, **8**, 751.